

NLO QCD+EW corrections to diphoton production in association with a vector boson

Nicolas Greiner,^a Marek Schönherr^{a,b}

^a*Physik Institut, Universität Zürich, Winterthurerstr.190, 8057 Zürich, Switzerland*

^b*Theoretical Physics Department, CERN, 1211 Geneva 23, Switzerland*

ABSTRACT: Processes with three external electroweak gauge bosons allow for a measurement of triple and quartic gauge couplings. They can be used to constrain anomalous gauge couplings, where new physics might predominantly couple to electroweak gauge bosons. In this paper we chose a class of such processes where we consider two photons and an additional vector boson in the final state. As additional vector boson we consider either a third photon or a W or Z boson. For the latter two cases we assume a leptonic decay of the boson. We calculate the next-to-leading order QCD and electroweak corrections to these processes with a particular emphasis on the until now unknown electroweak corrections. We find that the electroweak corrections to the total cross section are moderate in the range of a few per cent at most, but can reach several tens of per cent in regions of phase space that are particularly interesting in the context of new physics searches. In addition we investigate the difference between additive and multiplicative scheme when combining QCD and electroweak corrections and we assess the importance of photon induced contributions to these processes.

KEYWORDS: EW corrections, Photon, NLO, Jets

Contents

1	Introduction	1
2	Computational setup	2
3	Results	3
3.1	$\gamma\gamma\gamma$ production	5
3.2	$\gamma\gamma\ell\nu$ production	9
3.3	$\gamma\gamma\ell^+\ell^-$ production	12
4	Conclusions	15

1 Introduction

The precise understanding of the electroweak symmetry breaking mechanism is an important cornerstone of the LHC physics programme. Different realisations of the electroweak sector or new physics coupling to electroweak gauge bosons will yield to deviations compared to the Standard Model prediction. New physics effects can conveniently be described in terms of an effective theory where new heavy degrees of freedom are integrated out and deviations from the Standard Model are parametrised by higher dimensional operators [1, 2]. Higher dimensional operators can lead to deviations in triple and quartic gauge couplings. Moreover, new vertices (e.g. $\gamma\gamma\gamma$, $Z\gamma\gamma$) that do not exist in the Standard Model can appear. The class of processes that involve a pair of photons in association with another vector boson allows to measure deviations in triple and quartic gauge couplings and is therefore a particularly interesting class of processes. Consequently both ATLAS and CMS have measured these types of processes and derived constraints on anomalous gauge couplings [3–6].

In this paper we calculate the next-to-leading order QCD and electroweak corrections to the processes $\gamma\gamma\gamma$, $\gamma\gamma e^+e^-$ and $\gamma\gamma e^-\bar{\nu}_e$. For the latter two, all possible off-shell contributions of intermediate vector bosons are taken into account. The QCD corrections to these processes have already appeared in the literature [7–9]. For a more complete picture of the higher order effects we recompute them for a centre of mass energy of 13 TeV, and supplement them with the next-to-leading order electroweak corrections. Although the electroweak corrections are much smaller at the level of the total cross section compared to the NLO QCD corrections they are particularly important when deriving limits on anomalous couplings. The effects of higher dimensional operators increase in the high energy tails of differential distributions and lead to a change of the shapes. And it is in the same region where the Sudakov logarithms from the electroweak corrections will play an essential role as well.

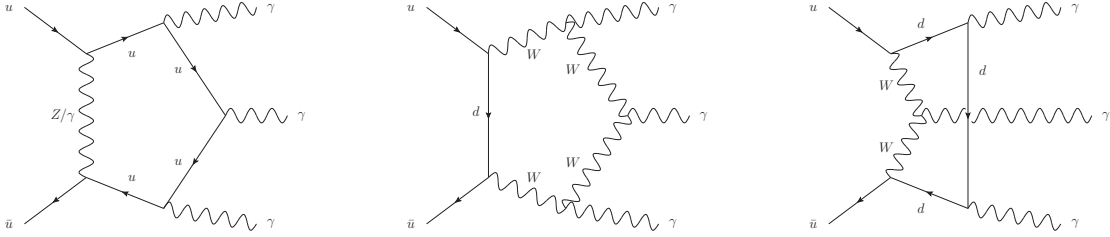


Figure 1: Sample diagrams of electroweak virtual corrections to triple photon production.

The paper is organized as follows. In Section 2 we describe the calculational setup that has been used to obtain our numerical result which we are going to discuss in Section 3 before we conclude in Section 4.

2 Calculational setup

The results presented in this paper have been obtained by combining the two tools GOSAM [10, 11] and SHERPA [12] which allows for a fully automated calculation of cross section and observables and next-to-leading order in QCD as well as in the electroweak coupling. GOSAM is a package which generates the code for the numerical evaluation of the one loop scattering amplitudes starting from the Feynman diagrams, generated with QGRAF [13] and further processed with FORM [14, 15] and SPINNEY [16] to perform necessary algebraic manipulations to obtain an optimized expression for the matrix elements. For the integrand reduction of the diagrams we use the NINJA library [17], an implementation of the technique of integrand reduction via Laurent expansion [18, 19]. Alternatively one can choose other reduction strategies such as OPP reduction method [20–22] which is implemented in d dimensions in SAMURAI [23], or methods based on tensor integral reduction as implemented in GOLEM95 [24–27]. We have used ONELOOP [28] to evaluate the scalar integrals.

A selection of one-loop amplitudes contributing to the three considered processes are shown in Figures 1–3. The highest point loop integrals occurring in $\gamma\gamma\gamma$ production are pentagons, while both $\gamma\gamma e^- \bar{\nu}_e$ and $\gamma\gamma e^+ e^-$ productions include up to hexagons at NLO EW.

SHERPA, on the other hand, provides the tree-level matrix elements, infrared subtraction, process management and phase-space integration of all contributions to all processes considered in this publication through its tree-level matrix element generator AMEGIC [29]. Its inbuilt infrared subtraction is performed in the QED generalisation of the Catani-Seymour scheme [30–36] and includes the appropriate initial state mass factorisation counter terms. Both programs, SHERPA and GOSAM, are interfaced through a dedicated interface based on the Binot Les Houches Accord [37, 38]. Cross-checks of the tree-level matrix elements of GOSAM and SHERPA and the renormalized pole coefficients of the virtual corrections of

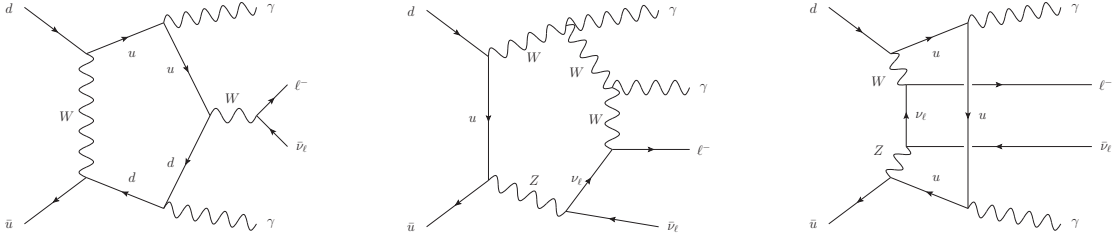


Figure 2: Sample diagrams of electroweak virtual corrections to diphoton production in association with a lepton-neutrino pair.

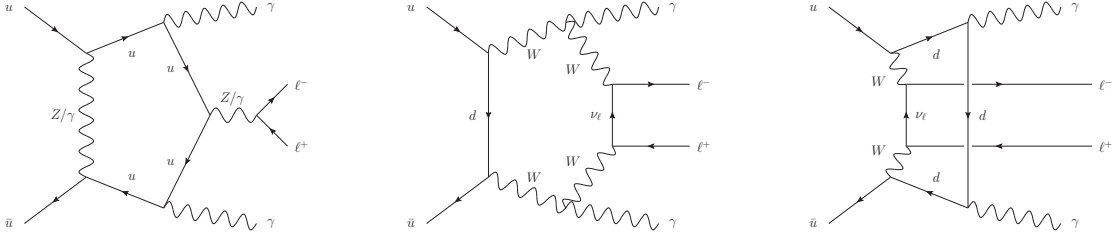


Figure 3: Sample diagrams of electroweak virtual corrections to diphoton production in association with a lepton-pair.

GOSAM and the infrared poles of SHERPA have been performed for several phase space points spanning multiple kinematic regimes and we have found excellent agreement.

This combination of tools was previously used to calculate the NLO QCD corrections to $ZZ + \text{jet}$, $t\bar{t} + 0, 1 \text{ jets}$, $W^+W^-b\bar{b}$ and $h + 0, 1, 2, 3 \text{ jets}$ production in [39–44] and the NLO EW corrections to $\gamma\gamma + 0, 1, 2 \text{ jets}$ production in [45].

3 Results

In this section we present numerical results for the NLO QCD and NLO EW corrections to all three production processes of a diphoton pair in association with a third vector boson, a third photon, a W or a Z boson, at the LHC at a centre-of-mass energy of 13 TeV. In case of an accompanying W or a Z boson, we consider the full off-shell leptonic final state, i.e. lepton-neutrino or lepton-pair production. All results are obtained in the Standard Model using the complex-mass scheme [46] with the following input parameters

$$\begin{aligned}
\alpha(0) &= 1/137.03599976 \\
G_\mu &= 1.1663787 \times 10^{-5} \text{ GeV}^2 \\
m_W &= 80.385 \text{ GeV} & \Gamma_W &= 2.085 \text{ GeV} \\
m_Z &= 91.1876 \text{ GeV} & \Gamma_Z &= 2.4952 \text{ GeV} \\
m_h &= 125.0 \text{ GeV} & \Gamma_h &= 0 \\
m_t &= 173.2 \text{ GeV} & \Gamma_t &= 0 .
\end{aligned}$$

While we calculate triple photon production in the $\alpha(0)$ -scheme, we use a mixed scheme for $\gamma\gamma W$ and $\gamma\gamma Z$ production: at LO two powers of α are taken in the $\alpha(0)$ -scheme, while one power of α is taken in the G_μ -scheme. The additional power of α in the NLO EW correction is evaluated in $\alpha(0)$ -scheme again. The virtual amplitudes are renormalised correspondingly. In all cases both the width of the top quark and the Higgs boson can safely be neglected as there are no diagrams containing either as s -channel propagators which can potentially go on-shell. All other lepton and parton masses and widths are set to zero, i.e. we are working in the five-flavour scheme. We use the CT14NLO PDF set with $\alpha_s(m_Z) = 0.118$ [47], interfaced through LHAPDF6 [48]. The use of a QCD-only PDF is justified by the fact that, at LO, the photon induced corrections are either non-existent ($\gamma\gamma\gamma$, $\gamma\gamma W$) or negligible ($\gamma\gamma Z$). This finding will be detailed in Section 3.3.

We define our central scales through

$$\mu_R^0 = \mu_F^0 = \frac{1}{2} H_T' . \quad (3.1)$$

In the case of the triple photon process H_T' is just given by the scalar sum of all final state transverse momenta, for the two processes with the massive vector bosons it is defined as

$$H_T' = E_T^V + \sum_{\gamma, q, g} p_{T,i} \quad (3.2)$$

with $E_T^{W^2} = (p_\ell + p_\nu)^2$ and $E_T^{Z^2} = (p_{\ell^+} + p_{\ell^-})^2$ in full analogy to the case of the case of vector boson production in association with jets [49]. As the Born process in each case has no μ_R dependence, we do not expect the choice of scale to have a significant influence on the size of the relative QCD and EW corrections. We calculate the leading order cross section $d\sigma_{\text{LO}}(\mu_F)$, which only depends on the factorisation scale μ_F , the NLO QCD differential correction factor $\delta_{\text{QCD}}(\mu_R, \mu_F)$, introducing the additional μ_R -dependence, and the NLO EW differential correction factor $\delta_{\text{EW}}(\mu_F^0)$. To estimate the impact of yet-to-be-calculated higher-order corrections we vary the free scales μ_R and μ_F by the conventional factor of two around their central values μ_R^0 and μ_F^0 , respectively. We do not vary the factorisation scale for the determination of δ_{EW} as the inherent, albeit normally phenomenologically irrelevant, stabilisation of the μ_F -dependence at NLO EW is not reflected in our chosen PDF. Hence,

	$pp \rightarrow \gamma\gamma\gamma$	$pp \rightarrow \gamma\gamma e^- \bar{\nu}_e$	$pp \rightarrow \gamma\gamma e^+ e^-$
σ_{LO} [fb]	$5.56^{+0.30}_{-0.36}$	$0.92^{+0.06}_{-0.07}$	$4.21^{+0.36}_{-0.41}$
δ_{QCD} [%] $p_{\text{T,jet}}^{\text{veto}} = \infty$	139^{+24}_{-27}	111^{+21}_{-24}	27^{+13}_{-18}
δ_{QCD} [%] $p_{\text{T,jet}}^{\text{veto}} = 30 \text{ GeV}$	35^{+7}_{-13}	41^{+8}_{-14}	19^{+11}_{-17}
δ_{EW} [%]	0.6	-1.8	-4.4

Table 1: Total cross sections at LO, NLO QCD and NLO EW for $\gamma\gamma\gamma$, $\gamma\gamma e^- \bar{\nu}_e$ and $\gamma\gamma e^+ e^-$ production at 13 TeV at the LHC.

our NLO EW result exhibits the exact same μ_{F} -dependence as the LO result. We define

$$\begin{aligned}
d\sigma_{\text{NLO QCD}} &= d\sigma_{\text{LO}} (1 + \delta_{\text{QCD}}) \\
d\sigma_{\text{NLO EW}} &= d\sigma_{\text{LO}} (1 + \delta_{\text{EW}}) \\
d\sigma_{\text{NLO QCD+EW}} &= d\sigma_{\text{LO}} (1 + \delta_{\text{QCD}} + \delta_{\text{EW}}) \\
d\sigma_{\text{NLO QCD}\times\text{EW}} &= d\sigma_{\text{LO}} (1 + \delta_{\text{QCD}}) (1 + \delta_{\text{EW}}) .
\end{aligned}
\tag{3.3}$$

Therein, the difference between NLO QCD+EW and NLO QCD \times EW, which is of relative $\mathcal{O}(\alpha_s\alpha)$, can serve as an indicator of the potential size of unknown corrections at that order.

In Table 1 we quote the inclusive cross sections for all three processes. The set of fiducial cuts for each process is detailed in its respective subsection below. We note that the NLO QCD corrections for both triple photon production and $\gamma\gamma W$ production are strongly jet veto dependent, a result that was previously discussed in great detail in [7, 9], and will be revisited in the following. A much milder jet veto dependence is found for $\gamma\gamma Z$ production. The electroweak corrections to inclusive cross sections are generally much smaller, ranging from 0.6% ($\gamma\gamma\gamma$) to -1.8% ($\gamma\gamma W$) and -4.4% ($\gamma\gamma Z$).

3.1 $\gamma\gamma\gamma$ production

The triple photon production process is defined by the presence of three identified photons in the central detector. To this end we use the smooth cone isolation criterion [50], limiting the amount of hadronic activity in a cone R_γ to

$$E_{\text{had,max}}(r_\gamma) = \epsilon p_{\text{T}}^\gamma \left(\frac{1 - \cos r_\gamma}{1 - \cos R_\gamma} \right)^n ,
\tag{3.4}$$

where r_γ denotes the angular separation between the photon and the parton, with

$$R_\gamma = 0.4 , \quad \epsilon = 0.05 , \quad n = 1 ,
\tag{3.5}$$

to define isolated photon candidates. These candidates are then ordered in transverse momentum. We require at least three such candidates within $|\eta| < 2.37$, the leading one of which needs $p_{\text{T}} > 40 \text{ GeV}$, while the all subleading ones need only $p_{\text{T}} > 30 \text{ GeV}$. Finally, a pairwise

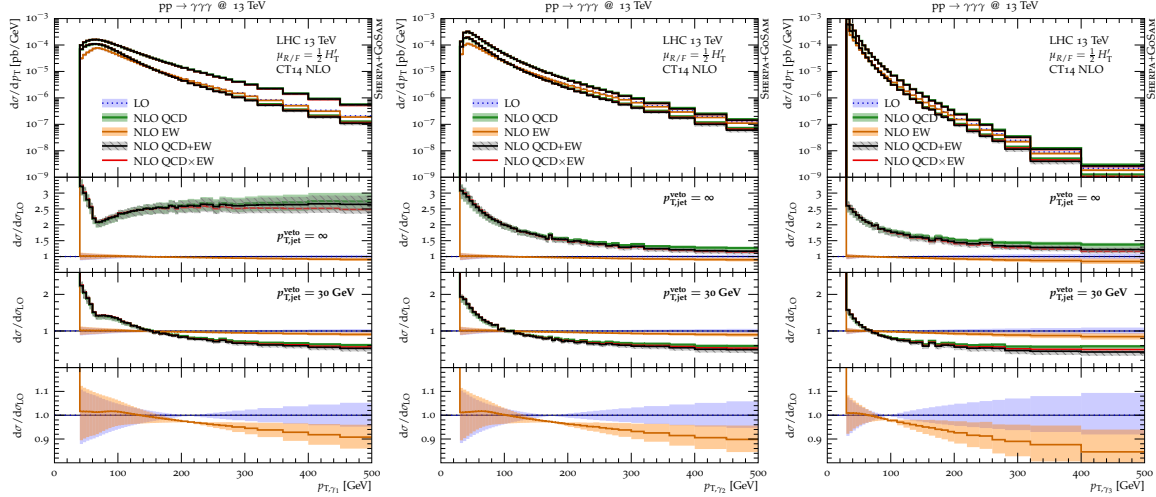


Figure 4: Transverse momentum of the leading (left), subleading (centre) and third leading (right) photon in triple photon production at the LHC at 13 TeV. The distributions are shown at LO (blue), NLO QCD (green), NLO EW (orange), NLO QCD+EW (black) and NLO QCD×EW (red) including scale uncertainties. The top panel displays the absolute predictions for both the case with and without the application of a jet veto of $p_{T,\text{jet}}^{\text{veto}} = 30$ GeV, the latter ones are easily recognisable due to their much reduced rate. The top ratio plot details the relative corrections to the leading order cross section without applying the jet veto, while the centre ratio plot applies the jet veto. The lower ratio highlights the size of the electroweak corrections.

separation of $\Delta R(\gamma_i, \gamma_j) > 0.4$ between all identified photons is required. It is worth noting that at NLO EW it is possible to find more than three isolated photons, in which case any combination may fulfill the above criteria.

Figure 4 displays the transverse momenta of the first three leading photons. The first observation is that, with the chosen set of cuts, the leading and subleading photon are of similar hardness, and generally much harder than the third leading photon. This suggests that we select primarily diphoton production events which is accompanied by a third, mostly bremsstrahlung, photon. The NLO QCD corrections exhibit a handful of interesting features. In the absence of a jet veto the fixed-order calculation exhibits huge correction factors, mainly induced by the opening of new channels in the real emission. Additionally, kinematic constraints present at LO¹ are released and lead to a larger phase space that can be populated. These findings mandate the inclusion of at least the $\gamma\gamma\gamma + \text{jet}$ production process at NLO QCD to arrive at a reliable description of inclusive $\gamma\gamma\gamma$ production, and thus either a NNLO QCD calculation or a multijet merging ansatz [34, 51]. While the inclusive QCD corrections

¹ At leading order the leading photon needs to be in a different hemisphere than both the subleading and third leading photon. Thus, $\Delta\phi_{\gamma_1\gamma_2}$ and $\Delta\phi_{\gamma_1\gamma_3}$ must be larger than $\frac{1}{2}\pi$.

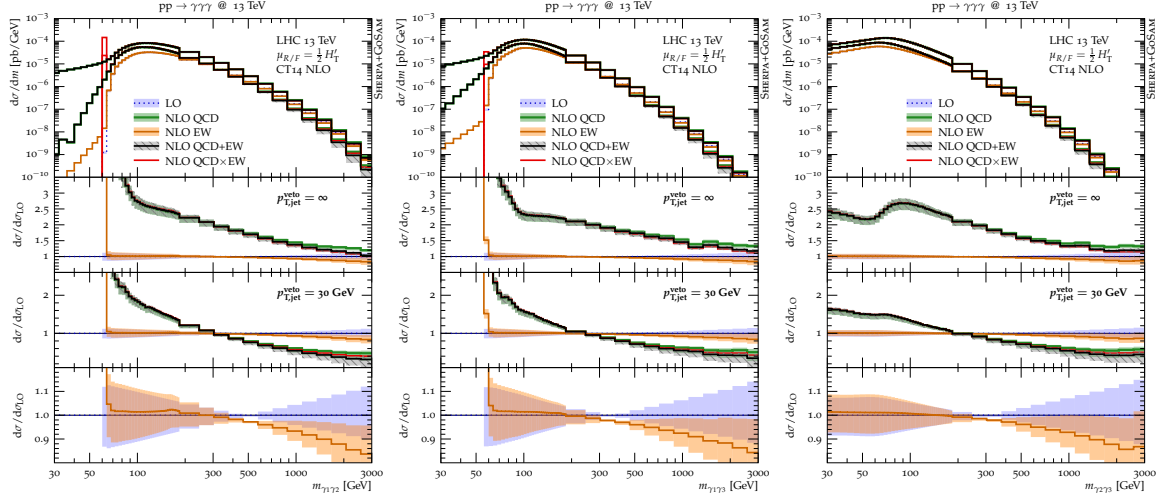


Figure 5: Pairwise invariant mass of the leading and subleading photon (left), leading and third leading photon (centre), subleading and third leading photon (right) in triple photon production at the LHC at 13 TeV. Details as in Fig. 4.

at very small transverse momenta are universally large for all three leading photon p_T -spectra ($\delta_{\text{QCD}} \approx 2$), they remain at exorbitantly large ($\delta_{\text{QCD}} \approx 1.5$) throughout the considered range only for the leading jet p_T . For both subleading photons the QCD corrections are quickly decreasing, leveling out at a approximately 20% at large transverse momenta. In the presence of a restrictive jet veto the very low transverse momentum region still experiences large correction of about $\delta_{\text{QCD}} \approx 1$. As transverse momenta are increasing, however, the QCD corrections now turn negative reaching now $-50 - 60\%$ and for all three photons.

The electroweak corrections, due to the absence of the opening of large new channels at the next-to-leading order, are dominated by the virtual corrections. Consequently, the release of the LO phase space restrictions in the real emission corrections only plays a minor role. For all three photons the electroweak corrections are small but positive at small transverse momenta and exhibit the usual Sudakov shape at large transverse momenta. They reach -10% for the leading and subleading photon and -20% for the third photon at $p_T = 500$ GeV. More importantly, beyond $p_T \gtrsim 170, 140$ and 80 GeV for the first, second and third leading photon, respectively, the electroweak corrections are not covered by the LO uncertainty estimate. Due to the different sizes of the QCD and electroweak corrections, the additive and multiplicative combination of corrections lead to very similar results.

Figure 5 continues with the three combinations of diphoton invariant masses. The p_T and ΔR requirements of the event selection induce a minimum in the distributions at leading order. The region below can only be filled if a fourth particle is present, as is the case in both the QCD and electroweak real emission corrections, leading to simultaneously huge corrections δ_{QCD} and δ_{EW} as the Born cross section vanishes. Due to this behaviour, the

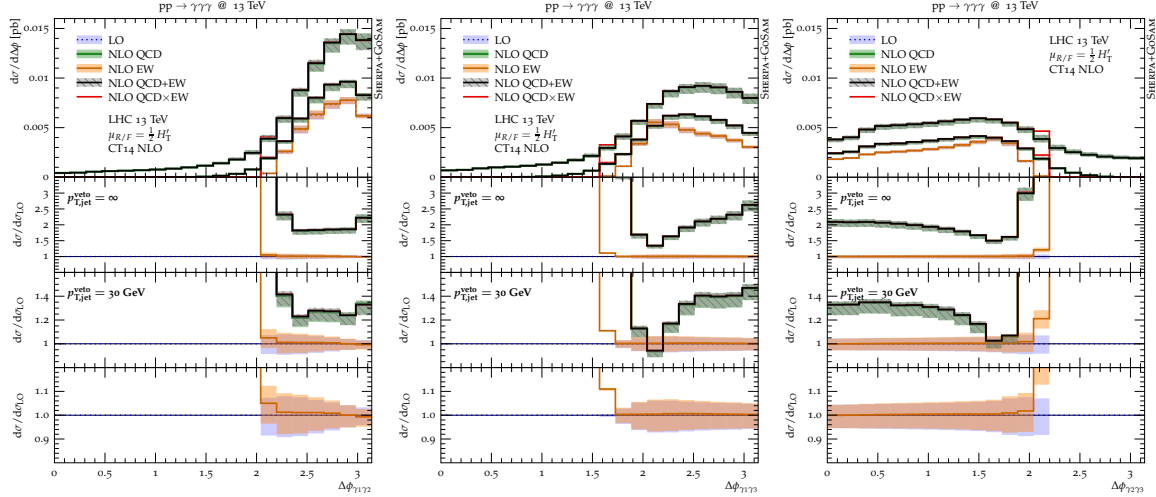


Figure 6: Azimuthal separation of the leading and subleading photon (left), leading and third leading photon (centre), subleading and third leading photon (right) in triple photon production at the LHC at 13 TeV. Details as in Fig. 4.

multiplicative combination of corrections, NLO QCD \times EW, ceases to be well defined and spikes in the distribution are visible. The distributions below, where $d\sigma_{LO} = 0$, are ill-defined. In consequence, for distributions where kinematic boundaries exist at leading order, but are lifted at higher orders, the multiplicative combination does not present a viable option for describing the observable throughout phase space.

The QCD corrections themselves again exceed 200% at small invariant masses, already well before the above described kinematic boundary effect takes hold. As the invariant masses are increasing, the QCD corrections are dropping to 20 – 30% for the inclusive selection. The structure the QCD corrections exhibit around 80-90 GeV in all three diphoton-pair invariant masses are induced by the acceptance cuts. In the presence of the jet veto, the QCD corrections are reduced and turn negative beyond $m_{\gamma\gamma} \gtrsim 300$ GeV reaching around -40% at 1 TeV. The electroweak corrections, on the other hand, are again moderate, ranging from $+1.5\%$ between 70 and 200 GeV for $m_{\gamma_1\gamma_2}$ and $m_{\gamma_1\gamma_3}$ and 0 and 100 GeV for $m_{\gamma_2\gamma_3}$. $m_{\gamma_1\gamma_2}$ exhibits a small rise in the correction at $2m_W$ due to resonant box diagrams in that region. This feature is also present in the electroweak corrections to diphoton production in this observable [45]. At large transverse momentum the usual Sudakov logarithms are recovered, resulting in corrections of around -8% at 1 TeV for all photon-pair invariant masses. Most importantly, beyond $m_{\gamma\gamma} \gtrsim 300$ GeV, the electroweak corrections are again not covered by the LO uncertainty estimate.

Finally, in Figure 6 we show the azimuthal separation $\Delta\phi$ between all three diphoton pairs. Similar features as before are visible as both the NLO QCD and NLO EW corrections relax the kinematic boundaries of the leading order calculation. Especially the azimuthal

separation of the leading and third leading photon receives substantial shape corrections throughout the entire spectrum, with and without the presence of a jet veto. The angular distribution between leading photon and the second or third subleading photon exhibit a kinematical edge at $\pi/2$ which is relaxed at NLO. This kinematical edge can be understood in the following way: Let us consider the first observable, the angular separation between the leading and the subleading photon, the argument also holds for the separation between the leading and the third leading photon. The third leading photon has to recoil against the system of the two leading photons. Let us go into the limit where the three photons have a very similar transverse momentum and consider the configuration where the leading photon is back-to-back to the third leading photon. Then the second photon must be perpendicular to this axis. If the third photon has less transverse momentum, it needs the second photon to recoil against the leading photon. Therefore it gets closer to the third photon and further away from the leading photon. $\pi/2$ is therefore the minimal distance the second photon can have to the leading one. Only at NLO where one can have additional radiation this constraint is relaxed. We will see later in Fig. 12 that this situation is also present when one replaces one of the subleading photons by a Z boson. The electroweak corrections are negligible for this observable.

3.2 $\gamma\gamma\ell\nu$ production

Next we move on to diphoton production in association with a W boson decaying leptonically. In this context, we will representatively focus on W^- bosons as we do not expect qualitatively different results for W^+ bosons. We define our fiducial phase space by following experimental setups [5]. First, we require the presence of exactly one charged lepton, dressed with all photons in a cone of size $R = 0.1$, with $p_T > 20$ GeV and $|\eta| < 2.5$. Among the remaining photons we require at least two identified ones, using the procedure described in Sec. 3.1, only changing the transverse momentum requirements to $p_T > 20$ GeV for both the leading and the subleading identified photon. We further demand the angular separation of both photons to be $\Delta R(\gamma_1, \gamma_2) > 0.4$ and each photon and the lepton to be $\Delta R(\ell, \gamma) > 0.7$. Furthermore we require the transverse mass of the lepton-neutrino system to be larger than 40 GeV. The inclusive cross sections and correction factors were detailed in Tab. 1.

Figure 7 shows the transverse momenta of the leading and subleading photon as well as the charged lepton. As was observed in triple photon production, the inclusive NLO QCD corrections are large. Nonetheless, they differ substantially between the three observables and in their different regions. While δ_{QCD} rises from values of 0.3 at small transverse momenta of the leading photon to 2 at $p_T \approx 100$ GeV, it remains constant above that value. In the subleading photon's transverse momentum, the situation is different. Experiencing an acceptance cut induced jump from 0.3 to 2.5 at low p_T , it decreases steadily thereafter to reach $\delta_{\text{QCD}} = 0.8$ at 500 GeV. The behaviour of the QCD corrections to the lepton p_T are then again qualitatively similar to that of the leading photon, starting at $\delta_{\text{QCD}} = 0.8$ at low p_T and rising steeply to 2.5 at 100 GeV and then gradually leveling out at 3.5. Again, the

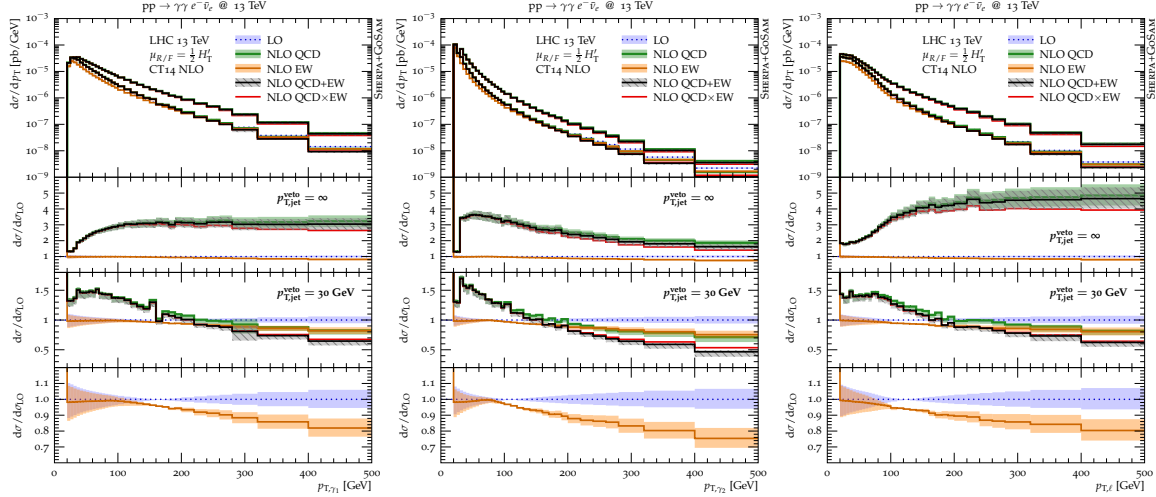


Figure 7: Transverse momentum of the leading (left), subleading (centre) and third leading (right) photon at the LHC at 13 TeV.

presence of a restrictive jet veto has little effect on the small transverse momentum regions, but effectively contains the size of the NLO QCD corrections to remain below $\delta_{\text{QCD}} = 0.5$. Instead, they are again driven negative, reaching $-20 - 30\%$ for all three observables.

The electroweak corrections are negative throughout, reaching -20% for the leading photon and the lepton and -25% for the subleading photon at 500 GeV. For this process, starting at transverse momenta of around 100 GeV, the electroweak corrections are much larger than the LO uncertainty estimate. Due to their larger size, as compared with the $\gamma\gamma$ production process, the difference between their additive and multiplicative combination with the QCD corrections becomes more pronounced when no jet veto is applied. One reason is that the QCD corrections are dominated by real emission contributions, which only receive the not-so-small electroweak correction factor in the multiplicative combination, but not the additive one. While this correction factor is, strictly speaking, associated only with the Born configuration, its application to real-emission configurations is well motivated in the electroweak Sudakov-regime at large transverse momenta. The concurrence of the additive and multiplicative schemes in the presence of the jet veto now precisely originates in the taming of the QCD corrections by restricting the influence of real-emission topologies.

Considering now the invariant mass of both photons and the leading photon and the lepton, presented in Figure 8, a similar picture presents itself. Both QCD corrections are moderate at small invariant masses and increase as the invariant mass rises. While $m_{\gamma_1\gamma_2}$ develops a correction factor of $\delta_{\text{QCD}} = 2$ at 200 GeV and then falls again to 0.4 at 1 TeV, $m_{\gamma_1\ell}$ only reaches a maximum of $\delta_{\text{QCD}} = 1.3$ before falling to 0.4 as well. In the presence of a jet veto, the shape of the corrections remains similar, but their magnitude is contained to be smaller than 0.5, turning negative around 500 GeV for both observables. The electroweak

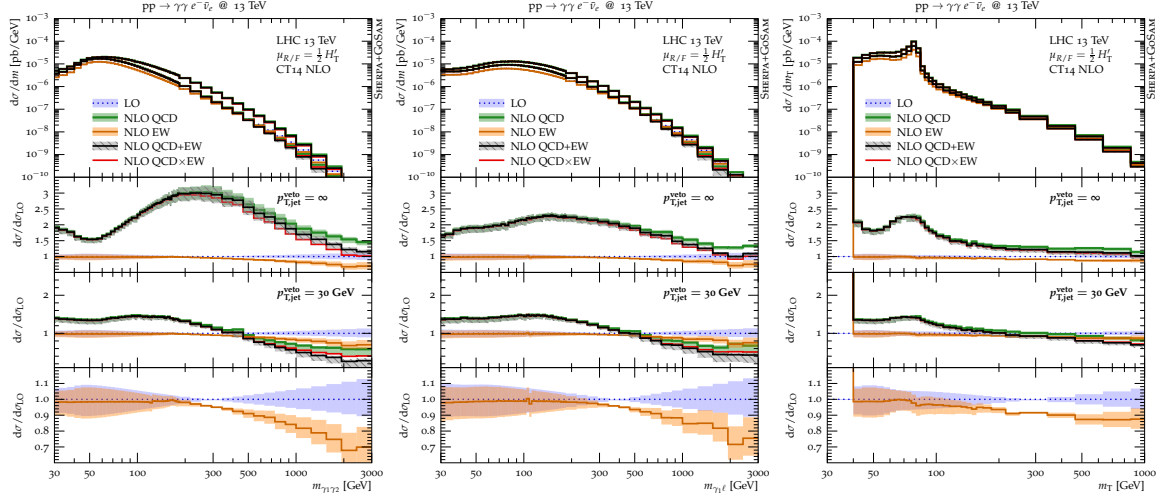


Figure 8: Pairwise invariant mass of the leading and subleading photon (left), leading and third leading photon (centre), subleading and third leading photon (right) at the LHC at 13 TeV.

corrections are again negative throughout, reaching $-15 - 20\%$ at invariant masses of 1 TeV. Again, above 200 GeV they are consistently outside the LO uncertainty estimate and play an important role.

Figure 8 also displays the transverse mass of the W boson on the right hand side. This distribution exhibits the general features known from inclusive W production, only the QCD corrections are scaled to the values present in this process. Electroweak corrections are less pronounced than for the invariant masses, but are still non-negligible. They reach about -8% at $m_T = 200$ GeV and -14% at 1 TeV.

Finally, Figure 9 presents the azimuthal separations of the leading and the subleading photon, and both the leading and subleading photon and the lepton. Contrary to $\gamma\gamma\gamma$ production, no kinematic constraints are present at LO, owing to the difference in flavour between the considered objects and the fact that the lepton is only one of two decay products of the W which takes the role of the third photon from point of view of the contributing diagrams. Both the QCD and EW corrections are generally flat, taking values of typically $\delta_{\text{QCD}} = 1 - 2$ in absence and $\delta_{\text{QCD}} = 0.4$ in presence of a jet veto, and $\delta_{\text{EW}} = -2\%$.

As none of the observables considered for this process exhibits a kinematic boundary at LO that is lifted at NLO, both the additive and the multiplicative combination of QCD and EW corrections present a viable prediction throughout and their difference can be taken as an indication of the potential size of higher-order corrections of $\mathcal{O}(\alpha_s\alpha)$.

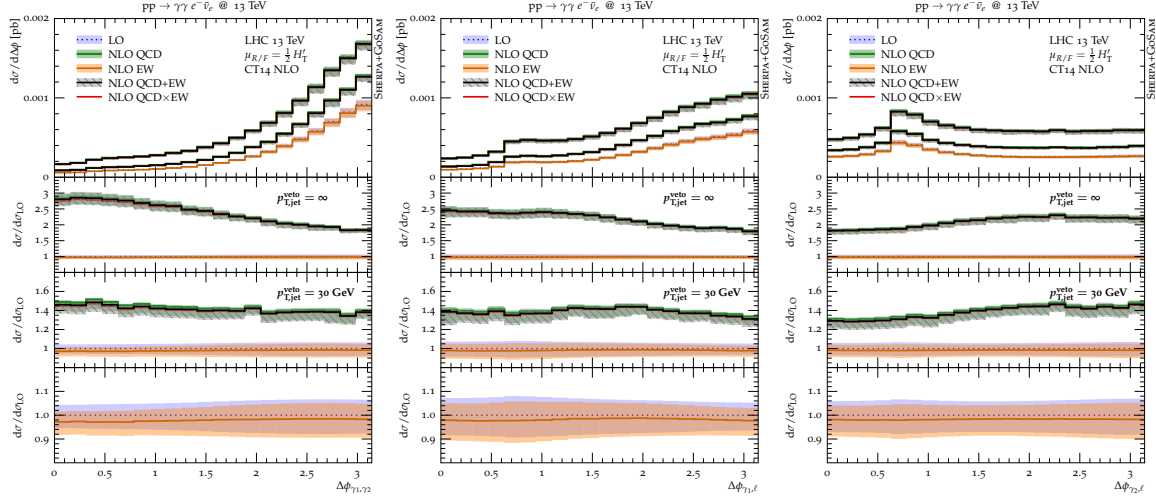


Figure 9: Azimuthal separation of the leading and subleading photon (left), leading and third leading photon (centre), subleading and third leading photon (right) at the LHC at 13 TeV.

3.3 $\gamma\gamma\ell^+\ell^-$ production

Finally, we consider diphoton production in association with a Z boson in its leptonic decay channel. In practise we look at lepton pair production including all non-resonant diagrams. The fiducial phase space of our analysis is defined as follows, again according to existing measurements [3]. First, we require the presence of exactly one lepton pair of opposite charge, dressed with all photons in a cone of size $R = 0.1$, with $p_T > 20$ GeV and $|\eta| < 2.47$. Their invariant mass must be larger than 40 GeV. As in the case of $\gamma\gamma W$ production, we then require at least two identified photons among the remaining ones after dressing, using the procedure described in Sec. 3.1, loosening the transverse momentum requirements to $p_T > 15$ GeV for both the leading and the subleading identified photon. We further demand the angular separation of both photons to be $\Delta R(\gamma_1, \gamma_2) > 0.4$ and each photon and the lepton to be $\Delta R(\ell, \gamma) > 0.4$. The inclusive cross sections and correction factors were detailed in Tab. 1.

In close analogy with the previous two processes considered, we start our discussion of the results with the transverse momenta of the leading and subleading photon and the charged lepton pair, cf. Figure 10. The first observation is, while the general behaviour of the spectra is the same as in $\gamma\gamma W$ production, the inclusive QCD corrections are much smaller in this case. They range between $\delta_{\text{QCD}} = 0.3 - 0.4$ for the leading and subleading photon and rise to 0.7 for the lepton pair at 500 GeV. The restrictive jet veto employed for the previous process reduces the QCD corrections further. Beyond the negligible impact at very small transverse momenta, they turn negative early on, reaching $\delta_{\text{QCD}} = -0.2 - 0.4$ at 500 GeV. The electroweak corrections are negative throughout, increasing from $\delta_{\text{EW}} = -4\%$ at low transverse momenta to -20% at 500 GeV. They are consistently larger than the LO

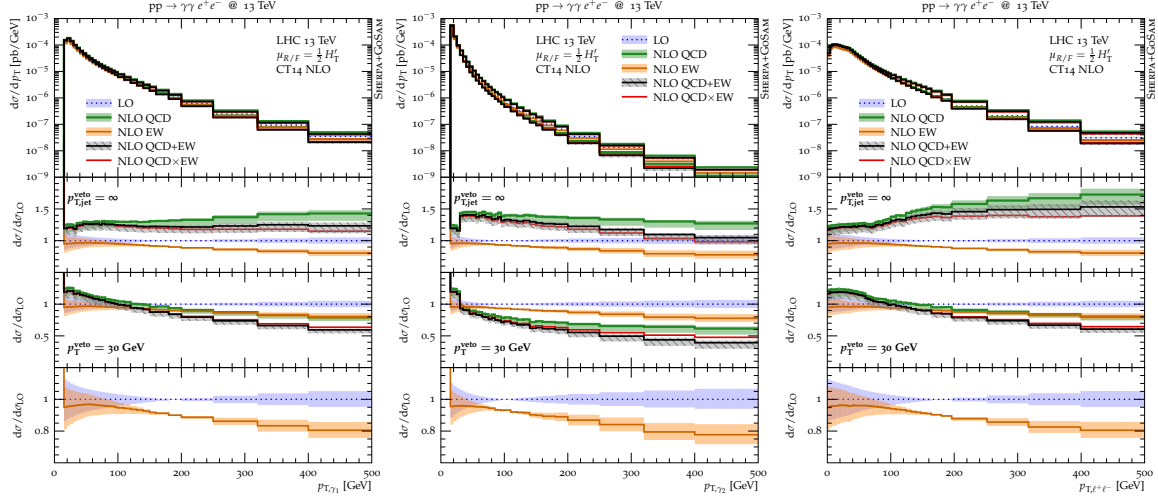


Figure 10: Transverse momentum of the leading (left) and subleading (centre) photon as well as the dressed lepton pair (right) in diphoton production in association with a lepton pair at the LHC at 13 TeV. Details as in Fig. 4.

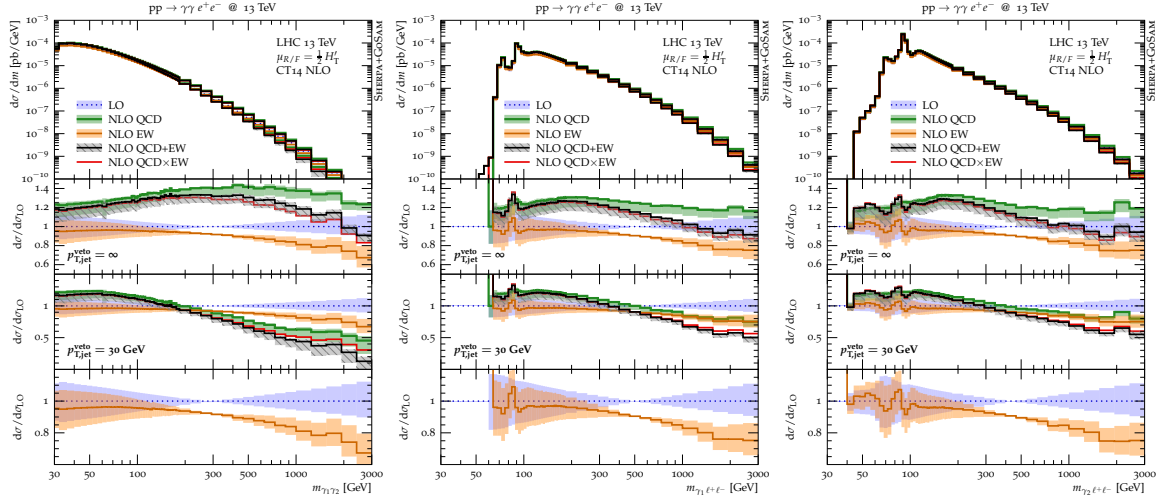


Figure 11: Pairwise invariant mass of the leading and subleading photon (left), the leading photon and the lepton pair (centre), and the subleading photon and the lepton pair (right) in diphoton production in association with a lepton pair at the LHC at 13 TeV. Details as in Fig. 4.

uncertainty estimate. As a consequence, the difference between the additive and multiplicative is comparably large, especially in the high p_T regions.

Figure 11 continues to display the invariant masses of the leading and subleading photon, and both the leading and subleading photon and the lepton pair. The familiar peak in $m_{\gamma_i \ell^+ \ell^-}$

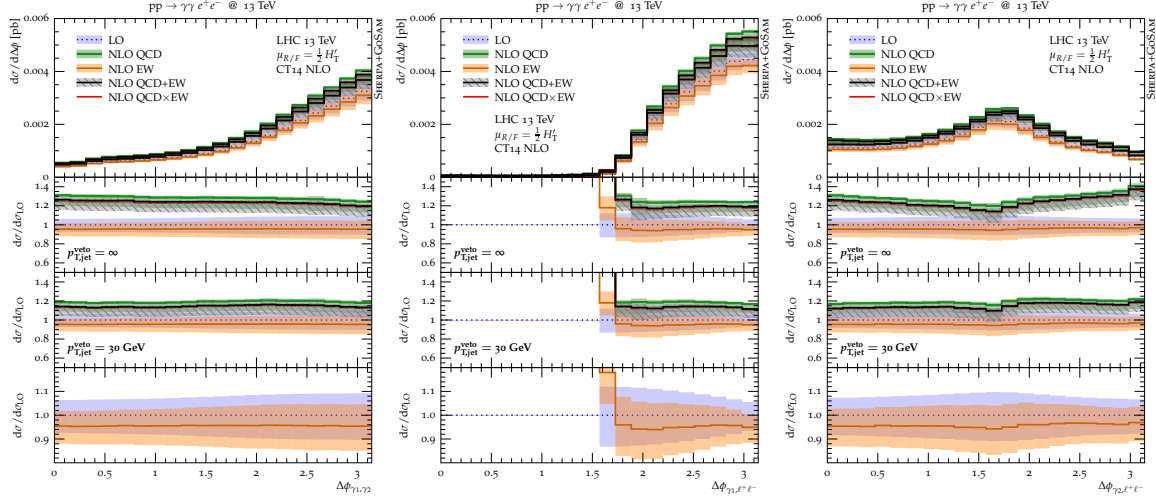


Figure 12: Azimuthal separation of the leading and subleading photon (left), the leading photon and the lepton pair (centre), and the subleading photon and the lepton pair (right) in diphoton production in association with a lepton pair at the LHC at 13 TeV. Details as in Fig. 4.

at the Z boson mass is produced by configurations where the respective photon is emitted by the lepton-pair from a resonant Z boson decay. Again, the QCD corrections are moderate, always staying below $\delta_{\text{QCD}} = 0.4$ and of a similar shape as encountered already in $\gamma\gamma W$ production. The jet veto again reduces the QCD corrections and drives them negative in large portions of the observable range, reaching as much as $\delta_{\text{QCD}} = -0.5$ for the diphoton invariant mass. The electroweak corrections, on the other hand, are qualitatively very similar to the $\gamma\gamma W$ case: with the exception of the well known positive radiative corrections below the Z peak, they are negative throughout, reaching $\delta_{\text{EW}} = -20\%$ at invariant masses of 1 TeV. As in the case of the transverse momenta, due to the similar size of the QCD and electroweak corrections at large transverse momenta, the difference between their additive and the multiplicative combination is amplified.

In Figure 12 we consider the azimuthal separation between the leading and subleading photon, and both the leading and subleading photon and the lepton pair. While both photons tend to be back-to-back, the azimuthal separation of the leading photon and the lepton pair exhibits a kinematic edge at LO, restricting it to be larger than $\frac{1}{2}\pi$. As discussed above this kinematic edge is also present in the case of the triple photon process (see Fig. 6) when considering the azimuthal angle between the leading and any subleading photon. On the contrary, the azimuthal separation of the subleading photon and the lepton pair exhibits no such limit at LO and instead peaks at roughly $\Delta\phi = \frac{1}{2}\pi$. The QCD corrections, with the exception of the aforementioned edge, are generally flat, taking values of $\delta_{\text{QCD}} \approx 0.3$ in the absence and $\delta_{\text{QCD}} \approx 0.2$ in the presence of a jet veto. The electroweak corrections are equally

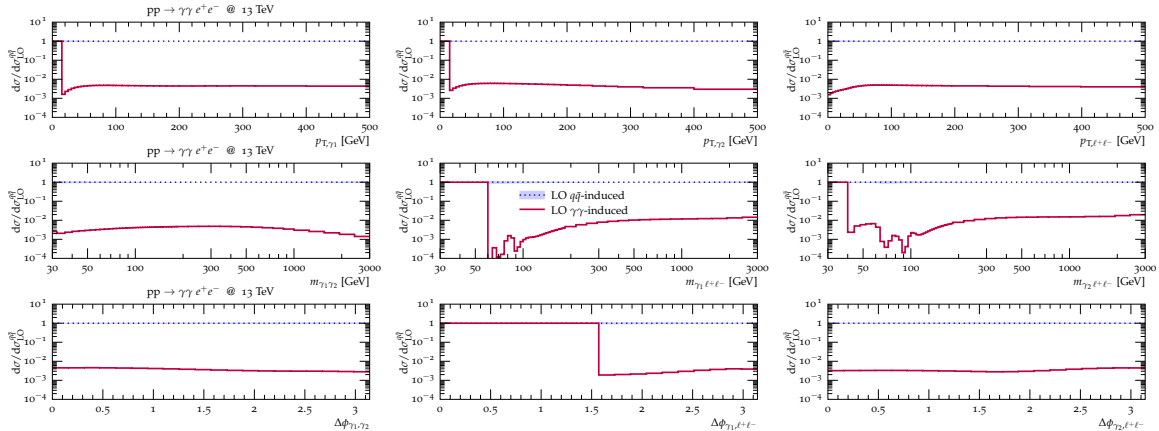


Figure 13: Contribution of $\gamma\gamma$ -induced production channels at LO.

flat and amount to $\delta_{\text{EW}} \approx -4\%$. Their additive and multiplicative combinations are very similar.

Finally, $\gamma\gamma Z$ production is the only process of the three processes considered in this publication which can be produced through photon-induced channels at leading order, $\gamma\gamma \rightarrow \ell^+\ell^-\gamma\gamma$. To this end, we investigate their contribution at LO in Figure 13. The photon-induced contribution is typically a few per mille of the LO cross section, but raises up to 2% for invariant masses larger than 1 TeV, especially $m_{\gamma_i\ell^+\ell^-}$. In this region, however, typical QCD and EW corrections are much larger such that this contribution can be safely ignored. As the photon-induced processes only contribute through non-resonant lepton-pair production, their contribution can be further suppressed by tightening the acceptance window in the lepton-pair invariant mass.

4 Conclusions

Processes that involve vertices of three and four electroweak gauge bosons are among the most promising processes where new physics might be found. Deviations from the Standard Model couplings or vertices that do not exist in the Standard Model might be found. The deviations from the Standard Model predictions can for instance conveniently be described by higher dimensional operators in terms of an effective field theory. Precise measurements of these processes allow to constrain and set limits to these higher dimensional operators.

In this paper we investigated the Standard Model predictions to a subset of such processes where we require two photons plus an additional electroweak vector boson in the final state. As additional vector boson we allowed for a third photon as well as for a W or Z boson where we considered their leptonic decay modes. This particularly implies that all off-shell and non-resonant contributions are taken into account.

We calculated the next-to-leading order QCD and electroweak corrections to these three processes for a set of realistic fiducial cuts. Particular emphasis has been put on the up to now unknown electroweak corrections as well as the combination of QCD and electroweak corrections with the aim of producing the most precise prediction possible within the Standard Model. As expected, we found the QCD corrections to be large and dominant compared to the electroweak corrections when calculating the corrections to the total cross sections. QCD corrections are particularly large for these processes due to new channels opening up at NLO but can effectively be reduced by applying a jet veto. Electroweak corrections lead to moderate corrections to the total cross section of up to 4.4% for the $\gamma\gamma\ell^+\ell^-$ process. However, in the high energy tail of differential distributions the electroweak corrections become increasingly important and can lead to corrections of up to 30%. Electroweak corrections become important in the same regions where one also expects increasing effects of higher dimensional operators. The precise determination of limits on higher dimensional operators therefore requires the inclusion of higher order correction of both QCD as well as of the electroweak interaction.

We also compared the two possibilities of combining QCD with electroweak corrections, namely either in an additive or in a multiplicative way. One expects that the difference between the two schemes is small as they can be seen as an estimation of neglected higher order contributions. We found that although this is true on the level of total cross sections there can be regions in phase space where the leading order contribution vanishes and therefore one or both K -factors become infinitely large. For those kinematical edges we observe a breakdown of the multiplicative scheme whereas the additive scheme provides a reliable estimation of the higher order uncertainties throughout the whole phase space.

Acknowledgements

N.G. was supported by the Swiss National Science Foundation under contract PZ00P2_154829. M.S. was supported by PITN-GA-2012-315877 (*MCnet*) and the ERC Advanced Grant MC@NNLO (340983).

References

- [1] S. Weinberg, *Phenomenological Lagrangians*, Physica **A96** (1979), [327–340](#).
- [2] S. Weinberg, *Conceptual Foundations of the Unified Theory of Weak and Electromagnetic Interactions*, Rev. Mod. Phys. **52** (1980), [515–523](#), [[Science210,1212\(1980\)](#)].
- [3] G. Aad et al., ATLAS collaboration, *Measurements of $Z\gamma$ and $Z\gamma\gamma$ production in pp collisions at $\sqrt{s} = 8$ TeV with the ATLAS detector*, Phys. Rev. **D93** (2016), no. 11, [112002](#), [[arXiv:1604.05232](#) [hep-ex]].

- [4] A. M. Sirunyan et al., CMS collaboration, *Measurements of the $pp \rightarrow W\gamma\gamma$ and $pp \rightarrow Z\gamma\gamma$ cross sections and limits on anomalous quartic gauge couplings at $\sqrt{s} = 8$ TeV*, JHEP **10** (2017), 072, [[arXiv:1704.00366](#) [hep-ex]].
- [5] G. Aad et al., ATLAS collaboration, *Evidence of $W\gamma\gamma$ Production in pp Collisions at $s=8$ TeV and Limits on Anomalous Quartic Gauge Couplings with the ATLAS Detector*, Phys. Rev. Lett. **115** (2015), no. 3, 031802, [[arXiv:1503.03243](#) [hep-ex]].
- [6] G. Aad et al., ATLAS collaboration, *Search for new phenomena in events with at least three photons collected in pp collisions at $\sqrt{s} = 8$ TeV with the ATLAS detector*, Eur. Phys. J. **C76** (2016), no. 4, 210, [[arXiv:1509.05051](#) [hep-ex]].
- [7] G. Bozzi, F. Campanario, M. Rauch and D. Zeppenfeld, *$Z\gamma\gamma$ production with leptonic decays and triple photon production at next-to-leading order QCD*, Phys. Rev. **D84** (2011), 074028, [[arXiv:1107.3149](#) [hep-ph]].
- [8] J. M. Campbell, H. B. Hartanto and C. Williams, *Next-to-leading order predictions for $Z\gamma$ +jet and $Z\gamma\gamma$ final states at the LHC*, JHEP **11** (2012), 162, [[arXiv:1208.0566](#) [hep-ph]].
- [9] G. Bozzi, F. Campanario, M. Rauch and D. Zeppenfeld, *$W^{+-}\gamma\gamma$ production with leptonic decays at NLO QCD*, Phys. Rev. **D83** (2011), 114035, [[arXiv:1103.4613](#) [hep-ph]].
- [10] G. Cullen, N. Greiner, G. Heinrich, G. Luisoni, P. Mastrolia, G. Ossola, T. Reiter and F. Tramontano, *Automated One-Loop Calculations with GoSam*, Eur. Phys. J. **C72** (2012), 1889, [[arXiv:1111.2034](#) [hep-ph]].
- [11] G. Cullen et al., *GOSAM-2.0: a tool for automated one-loop calculations within the Standard Model and beyond*, Eur. Phys. J. **C74** (2014), no. 8, 3001, [[arXiv:1404.7096](#) [hep-ph]].
- [12] T. Gleisberg, S. Höche, F. Krauss, M. Schönherr, S. Schumann, F. Siegert and J. Winter, *Event generation with SHERPA 1.1*, JHEP **02** (2009), 007, [[arXiv:0811.4622](#) [hep-ph]].
- [13] P. Nogueira, *Automatic Feynman graph generation*, J. Comput. Phys. **105** (1993), 279–289.
- [14] J. A. M. Vermaseren, *New features of FORM*, [arXiv:math-ph/0010025](#) [math-ph].
- [15] J. Kuipers, T. Ueda, J. A. M. Vermaseren and J. Vollinga, *FORM version 4.0*, Comput. Phys. Commun. **184** (2013), 1453–1467, [[arXiv:1203.6543](#) [cs.SC]].
- [16] G. Cullen, M. Koch-Janusz and T. Reiter, *Spinney: A Form Library for Helicity Spinors*, Comput. Phys. Commun. **182** (2011), 2368–2387, [[arXiv:1008.0803](#) [hep-ph]].

- [17] T. Peraro, *Ninja: Automated Integrand Reduction via Laurent Expansion for One-Loop Amplitudes*, Comput. Phys. Commun. **185** (2014), 2771–2797, [[arXiv:1403.1229](#) [hep-ph]].
- [18] P. Mastrolia, E. Mirabella and T. Peraro, *Integrand reduction of one-loop scattering amplitudes through Laurent series expansion*, JHEP **06** (2012), 095, [[arXiv:1203.0291](#) [hep-ph]], [Erratum: JHEP11,128(2012)].
- [19] H. van Deurzen, G. Luisoni, P. Mastrolia, E. Mirabella, G. Ossola and T. Peraro, *Multi-leg One-loop Massive Amplitudes from Integrand Reduction via Laurent Expansion*, JHEP **03** (2014), 115, [[arXiv:1312.6678](#) [hep-ph]].
- [20] G. Ossola, C. G. Papadopoulos and R. Pittau, *Reducing full one-loop amplitudes to scalar integrals at the integrand level*, Nucl. Phys. **B763** (2007), 147–169, [[arXiv:hep-ph/0609007](#) [hep-ph]].
- [21] P. Mastrolia, G. Ossola, C. G. Papadopoulos and R. Pittau, *Optimizing the Reduction of One-Loop Amplitudes*, JHEP **06** (2008), 030, [[arXiv:0803.3964](#) [hep-ph]].
- [22] G. Ossola, C. G. Papadopoulos and R. Pittau, *On the Rational Terms of the one-loop amplitudes*, JHEP **05** (2008), 004, [[arXiv:0802.1876](#) [hep-ph]].
- [23] P. Mastrolia, G. Ossola, T. Reiter and F. Tramontano, *Scattering AMplitudes from Unitarity-based Reduction Algorithm at the Integrand-level*, JHEP **08** (2010), 080, [[arXiv:1006.0710](#) [hep-ph]].
- [24] G. Heinrich, G. Ossola, T. Reiter and F. Tramontano, *Tensorial Reconstruction at the Integrand Level*, JHEP **10** (2010), 105, [[arXiv:1008.2441](#) [hep-ph]].
- [25] T. Binoth, J. P. Guillet, G. Heinrich, E. Pilon and T. Reiter, *Golem95: A Numerical program to calculate one-loop tensor integrals with up to six external legs*, Comput. Phys. Commun. **180** (2009), 2317–2330, [[arXiv:0810.0992](#) [hep-ph]].
- [26] G. Cullen, J. P. Guillet, G. Heinrich, T. Kleinschmidt, E. Pilon, T. Reiter and M. Rodgers, *Golem95C: A library for one-loop integrals with complex masses*, Comput. Phys. Commun. **182** (2011), 2276–2284, [[arXiv:1101.5595](#) [hep-ph]].
- [27] J. P. Guillet, G. Heinrich and J. F. von Soden-Fraunhofen, *Tools for NLO automation: extension of the golem95C integral library*, Comput. Phys. Commun. **185** (2014), 1828–1834, [[arXiv:1312.3887](#) [hep-ph]].
- [28] A. van Hameren, *OneLoop: For the evaluation of one-loop scalar functions*, Comput. Phys. Commun. **182** (2011), 2427–2438, [[arXiv:1007.4716](#) [hep-ph]].
- [29] F. Krauss, R. Kuhn and G. Soff, *AMEGIC++ 1.0: A Matrix element generator in C++*, JHEP **02** (2002), 044, [[arXiv:hep-ph/0109036](#) [hep-ph]].
- [30] S. Catani and M. H. Seymour, *A General algorithm for calculating jet cross-sections in*

- NLO QCD*, Nucl. Phys. **B485** (1997), 291–419, [[arXiv:hep-ph/9605323](#) [hep-ph]], [Erratum: Nucl. Phys. **B510**, 503(1998)].
- [31] S. Dittmaier, *A General approach to photon radiation off fermions*, Nucl. Phys. **B565** (2000), 69–122, [[arXiv:hep-ph/9904440](#) [hep-ph]].
- [32] T. Gleisberg and F. Krauss, *Automating dipole subtraction for QCD NLO calculations*, Eur. Phys. J. **C53** (2008), 501–523, [[arXiv:0709.2881](#) [hep-ph]].
- [33] S. Kallweit, J. M. Lindert, P. Maierhöfer, S. Pozzorini and M. Schönherr, *NLO electroweak automation and precise predictions for W +multijet production at the LHC*, JHEP **04** (2015), 012, [[arXiv:1412.5157](#) [hep-ph]].
- [34] S. Kallweit, J. M. Lindert, P. Maierhöfer, S. Pozzorini and M. Schönherr, *NLO QCD+EW predictions for V + jets including off-shell vector-boson decays and multijet merging*, JHEP **04** (2016), 021, [[arXiv:1511.08692](#) [hep-ph]].
- [35] S. Kallweit, J. M. Lindert, S. Pozzorini and M. Schönherr, *NLO QCD+EW predictions for $2\ell 2\nu$ diboson signatures at the LHC*, [arXiv:1705.00598](#) [hep-ph].
- [36] M. Schönherr, In preparation.
- [37] T. Binoth et al., *A Proposal for a standard interface between Monte Carlo tools and one-loop programs*, Comput. Phys. Commun. **181** (2010), 1612–1622, [[arXiv:1001.1307](#) [hep-ph]], [1(2010)].
- [38] S. Alioli et al., *Update of the Binoth Les Houches Accord for a standard interface between Monte Carlo tools and one-loop programs*, Comput. Phys. Commun. **185** (2014), 560–571, [[arXiv:1308.3462](#) [hep-ph]].
- [39] T. Binoth, T. Gleisberg, S. Karg, N. Kauer and G. Sanguinetti, *NLO QCD corrections to ZZ + jet production at hadron colliders*, Phys. Lett. **B683** (2010), 154–159, [[arXiv:0911.3181](#) [hep-ph]].
- [40] S. Höche, J. Huang, G. Luisoni, M. Schönherr and J. Winter, *Zero and one jet combined next-to-leading order analysis of the top quark forward-backward asymmetry*, Phys. Rev. **D88** (2013), no. 1, 014040, [[arXiv:1306.2703](#) [hep-ph]].
- [41] N. Greiner, S. Höche, G. Luisoni, M. Schönherr, J.-C. Winter and V. Yundin, *Phenomenological analysis of Higgs boson production through gluon fusion in association with jets*, JHEP **01** (2016), 169, [[arXiv:1506.01016](#) [hep-ph]].
- [42] N. Greiner, S. Höche, G. Luisoni, M. Schönherr and J.-C. Winter, *Full mass dependence in Higgs boson production in association with jets at the LHC and FCC*, JHEP **01** (2017), 091, [[arXiv:1608.01195](#) [hep-ph]].
- [43] G. Heinrich, A. Maier, R. Nisius, J. Schlenk and J. Winter, *NLO QCD corrections to $W^+W^-b\bar{b}$ production with leptonic decays in the light of top quark mass and asymmetry measurements*, JHEP **06** (2014), 158, [[arXiv:1312.6659](#) [hep-ph]].

- [44] G. Heinrich, A. Maier, R. Nisius, J. Schlenk, M. Schulze, L. Scyboz and J. Winter, *NLO and off-shell effects in top quark mass determinations*, [arXiv:1709.08615](#) [hep-ph].
- [45] M. Chiesa, N. Greiner, M. Schönherr and F. Tramontano, *Electroweak corrections to diphoton plus jets*, [arXiv:1706.09022](#) [hep-ph].
- [46] A. Denner, S. Dittmaier, M. Roth and L. H. Wieders, *Electroweak corrections to charged-current $e^+ e^- \rightarrow 4$ fermion processes: Technical details and further results*, Nucl. Phys. **B724** (2005), 247–294, [[arXiv:hep-ph/0505042](#) [hep-ph]], [Erratum: Nucl. Phys. B854,504(2012)].
- [47] S. Dulat, T.-J. Hou, J. Gao, M. Guzzi, J. Huston, P. Nadolsky, J. Pumplin, C. Schmidt, D. Stump and C. P. Yuan, *New parton distribution functions from a global analysis of quantum chromodynamics*, Phys. Rev. **D93** (2016), no. 3, 033006, [[arXiv:1506.07443](#) [hep-ph]].
- [48] A. Buckley, J. Ferrando, S. Lloyd, K. Nordström, B. Page, M. Rfenacht, M. Schnherr and G. Watt, *LHAPDF6: parton density access in the LHC precision era*, Eur. Phys. J. **C75** (2015), 132, [[arXiv:1412.7420](#) [hep-ph]].
- [49] C. F. Berger, Z. Bern, L. J. Dixon, F. Febres Cordero, D. Forde, T. Gleisberg, H. Ita, D. A. Kosower and D. Maitre, *Next-to-Leading Order QCD Predictions for $W+3$ -Jet Distributions at Hadron Colliders*, Phys. Rev. **D80** (2009), 074036, [[arXiv:0907.1984](#) [hep-ph]].
- [50] S. Frixione, *Isolated photons in perturbative QCD*, Phys. Lett. **B429** (1998), 369–374, [[arXiv:hep-ph/9801442](#) [hep-ph]].
- [51] S. Hoeche, F. Krauss, M. Schonherr and F. Siegert, *QCD matrix elements + parton showers: The NLO case*, JHEP **04** (2013), 027, [[arXiv:1207.5030](#) [hep-ph]].